Received: 18 September 2023 | Revised: 19 December 2023 | Accepted: 22 December 2023

DOI: 10.1002/hyp.15078

RESEARCH ARTICLE

WILEY

Water-rock interactions drive chemostasis

Sara Warix[1] | Alexis Navarre-Sitchler[1,2] | Kamini Singha[1,2]

[1]Hydrologic Science and Engineering Program, Colorado School of Mines, Golden, Colorado, USA

[2]Geology and Geological Engineering Department, Colorado School of Mines, Golden, Colorado, USA

Correspondence
Sara Warix, Hydrologic Science and Engineering Program, Colorado School of Mines, Golden, CO, USA.
Email: swarix@mines.edu

Funding information
National Science Foundation

Abstract

The western U.S. is experiencing shifts in recharge due to climate change, and it is currently unclear how hydrologic shifts will impact geochemical weathering and stream concentration–discharge (*C*–*Q*) patterns. Hydrologists often use *C*–*Q* analyses to assess feedbacks between stream discharge and geochemistry, given abundant stream discharge and chemistry data. Chemostasis is commonly observed, indicating that geochemical controls, rather than changes in discharge, are shaping stream *C*–*Q* patterns. However, few *C*–*Q* studies investigate how geochemical reactions evolve along groundwater flowpaths before groundwater contributes to streamflow, resulting in potential omission of important *C*–*Q* controls such as coupled mineral dissolution and clay precipitation and subsequent cation exchange. Here, we use field observations—including groundwater age, stream discharge, and stream and groundwater chemistry—to analyse *C*–*Q* relations in the Manitou Experimental Forest in the Colorado Front Range, USA, a site where chemostasis is observed. We combine field data with laboratory analyses of whole rock and clay x-ray diffraction and soil cation-extraction experiments to investigate the role that clays play in influencing stream chemistry. We use Geochemist's Workbench to identify geochemical reactions driving stream chemistry and subsequently suggest how climate change will impact stream *C*–*Q* trends. We show that as groundwater age increases, *C*–*Q* slope and stream solute response are not impacted. Instead, primary mineral dissolution and subsequent clay precipitation drive strong chemostasis for silica and aluminium and enable cation exchange that buffers calcium and magnesium concentrations, leading to weak chemostatic behaviour for divalent cations. The influence of clays on stream *C*–*Q* highlights the importance of delineating geochemical controls along flowpaths, as upgradient mineral dissolution and clay precipitation enable downgradient cation exchange. Our results suggest that geochemical reactions will not be impacted by future decreasing flows, and thus where chemostasis currently exists, it will continue to persist despite changes in recharge.

KEYWORDS
cation exchange, chemostasis, climate change, concentration-discharge, groundwater, groundwater age, surface water, water-rock interaction

1 | INTRODUCTION

Climate change is expected to alter the timing, magnitude, and phase of recharge by the latter half of the 21st century. Warmer temperatures will increase the elevation of the rain-snow transition in mountainous regions (Hotovy et al., 2023; Meixner et al., 2016), thus shifting the primary form of winter precipitation (Klos et al., 2014) and altering groundwater flowpaths (e.g., Fang et al., 2019) with unknown implications for stream hydrology and chemistry. To predict how stream solute fluxes might shift in future climate scenarios, we must

be able to explain the relation between hydrologic fluxes and geochemical reactions that drive solute concentrations in water sourcing streams. Headwater streams are of particular interest as they comprise over 50% of the global river network (Datry et al., 2011) and accumulate solutes that eventually contribute to downstream water resources and influence geochemical reactions (Wondzell, 2011).

Concentration–discharge (*C*–*Q*) plots and the slopes from those log–log plots are a common way to explore the feedback between hydrologic and geochemical fluxes in surface water (Chorover et al., 2017; Wymore et al., 2023) because of the ease in which *C*–*Q* plots are made as a result of readily available discharge and chemistry data. Such plots can be used to make inferences about streamflow source (Evans & Davies, 1998), geochemical reactions (Li et al., 2017), and hydrologic connection (Knapp et al., 2022). For example, during high flows, a negative slope may exist, where solute concentrations decrease due to dilution from snowmelt or other young water. High flows may also cause stagnant dissolved solutes to mobilize, leading to high solute concentrations and a positive slope. Streams may also exhibit chemostasis, or no notable slope between log(concentration) and log(discharge), when stream solute concentrations remain constant despite variable discharge. The horizontal slope associated with chemostasis inherently shows that discharge is not the primary control on solute concentration variability in streams—rather, stream chemistry has been hypothesized to be driven by geochemical reactions that control groundwater chemistry (Li et al., 2017; Zhi et al., 2019) and the hydrologic connection between solute source and active surface flows (Knapp et al., 2022). For example, during high-flow events, subsurface waters with high-enough solute concentrations to maintain stream solute concentrations become connected to the stream (Li et al., 2017).

Hydrologists have long attempted to understand drivers of chemostasis (Johnson et al., 1969) as it has been ubiquitously observed in catchments throughout the U.S. despite diversity in catchment size, geology, and topography (Godsey et al., 2009). However, despite the large number of *C*–*Q* studies, few investigate how the geochemical processes that shape groundwater chemistry evolve along flowpaths before contributing to streamflow. For example, many *C*–*Q* studies have report chemostasis for both $SiO_{2(aq)}$ and/or Al^{3+} as well as still chemostatic but slightly more negative *C*–*Q* slopes for Ca^{2+} and/or Mg^{2+} for a variety of catchments (Conroy et al., 2022; Godsey et al., 2009, 2019; Herndon et al., 2015; Kim et al., 2017), highlighting the potential for geochemical reactions to impact individual solutes differently. Here, we investigate the coupled geochemical reactions that happen along groundwater flowpaths, including (1) primary mineral dissolution leading to (2) clay precipitation and (3) subsequent cation-exchange reactions. Identification and parsing of geochemical reactions allows us to quantify how groundwater geochemistry evolves along flowpaths before sourcing stream solutes, and subsequently, how stream chemistry may change under future climate.

The age of groundwater sourcing streamflow can vary by orders of magnitude (Carroll et al., 2020) and is expected to increase as climate change alters recharge patterns (Manning et al., 2012; Segura, 2021), increasing the time available for rock weathering and geochemical reactions in the subsurface. Groundwater solute concentrations have been observed to increase with groundwater age as solute concentrations increase where groundwater spends longer in the subsurface weathering material (Beisner et al., 2020; Genereux et al., 2009; Rademacher et al., 2001). However, because mineral-dissolution and precipitation reactions are time dependent, to predict how groundwater geochemistry may shift under future climate we must be able to identify how long groundwater spends in the subsurface with potential to weather rocks. Where flowpaths are long and groundwater age is old, groundwater is often at or near geochemical equilibrium, causing groundwater-solution concentrations to be constant as controlled by the reactions at equilibrium (Maher, 2011; Torres et al., 2015; Winnick & Maher, 2018). Long flowpaths enable weathering of primary silicate minerals formed during rock crystallization so that groundwater approaches geochemical saturation and drives precipitation of secondary minerals, such as clays. Clay precipitation is often slow enough to limit primary silicate dissolution by maintaining slightly geochemically undersaturated conditions for primary silicate minerals while also sustaining oversaturation of the clay phases (Maher et al., 2009). This idea was suggested by the "slow clay hypothesis" in Maher et al. (2006), which shows that slow clay-precipitation rates enable porewater to approach equilibrium with respect to plagioclase because its dissolution rate is buffered by the uptake of $SiO_{2(aq)}$ and Al^{3+} in clays. In addition, fast geochemical-reaction rates relative to water-transit times can cause transport-limited weathering, where additional weathering is limited by precipitated material that blocks fresh reaction faces, such as in fractured-granite systems (Andrews & Navarre-Sitchler, 2021). These transport-limited settings enable bedrock weathering in conditions close to geochemical equilibrium to drive stream chemostasis because fresh rock faces are not quickly exposed to circulating groundwater due to the presence of clays. After clays precipitate, kinetically fast cation-exchange reactions on clays can buffer positively charged ions in solution (Gooseff et al., 2004; Hoagland et al., 2017). Clays can impact base-cation (Ca^{2+}, Mg^{2+}, Na^{+}, and K^{+}) concentrations through incorporation of cations into the crystal structure and/or cation exchange on charged clay surfaces. When divalent cations occupy cation-exchange sites on clay surfaces (Langmuir, 1997), rapid cation exchange between fluids and clay surfaces (seconds to minutes; Malcolm & Kennedy, 1969) can buffer cation ratios in the fluid. Some clays such as montmorillonites and vermiculites have higher capacity to exchange cations than other clays (e.g. chlorite, kaolinite, etc.) (Drever, 1998), highlighting the importance of local geology and upgradient dissolution reactions in regulating in-stream geochemical reactions.

Quantifying the role that cation exchange plays in modulating stream chemistry is important as cation exchange can buffer stream-cation concentrations and influence downgradient geochemical reactions and stream chemistry (Capuano & Jones, 2020; Eeman et al., 2017; Kim et al., 2017). Despite the geologic pervasiveness of clays, the role that cation exchange plays in influencing stream *C*–*Q* patterns and subsequent impacts on downstream water quality in headwater streams is not commonly included in studies investigating drivers of chemostasis. Li et al. (2017) simulated that where groundwater sources streams, increased cation exchange capacity causes a shift towards more dilutive behaviour for Mg^{2+}, highlighting the

potential importance of clays in regulating stream chemistry. Limited field work shows that in both an alpine catchment in Colorado (Clow & Mast, 2010) and at the Shale Hills Critical Zone Observatory in Pennsylvania (Herndon et al., 2015; Hoagland et al., 2017), rain and snow contribute protons to groundwater that quickly exchange for cations in the exchange pool, causing cation exchange to be an important secondary control on stream chemostasis, preceded by primary mineral dissolution and secondary mineral precipitation. While these studies have begun to highlight the importance of cation exchange in driving stream chemostasis, they represent the extent of work done, despite decades of *C*–*Q* literature. It is also currently unclear whether stream chemostasis driven by cation exchange will persist with changes in climate and recharge patterns.

Here, we seek to identify mechanisms controlling stream-water chemistry and *C*–*Q* patterns and predict future geochemical resilience by exploring the geochemical reactions that control surface chemistry in a montane headwater stream. In Warix et al. (2023), we investigated hydrologic resilience at the Manitou Experimental Forest, a small (3 km^2) montane headwater catchment located near the Colorado Front Range, by identifying how topography and geology impact groundwater age and groundwater-surface water connection. In this paper, we seek to build off that hydrologic foundation by investigating geochemical resilience in the same watershed. Specifically, we explore the connection between groundwater age and drivers of stream chemistry and *C*–*Q* patterns at eight sites throughout Manitou that exhibit chemostasis and are predominantly supported by old groundwater year-round. We use *C*–*Q* patterns to couple hydrologic and geochemical fluxes, trace the geochemical evolution of groundwater, and identify drivers of stream solute concentrations and how controls may shift with climate. We ask: (1) Is groundwater sufficiently old enough for geochemical equilibrium to drive chemostasis? (2) What is the relative importance of clay precipitation and subsequent cation exchange reactions in regulating stream chemostasis? And (3) How will *C*–*Q* patterns shift in response to future changes in recharge patterns? We hypothesize that old, geochemically-evolved water precipitating clays is the driver of chemostasis for $SiO_{2(aq)}$ and Al^{3+}, and that cation exchange is a secondary control on Ca^{2+} and Mg^{2+} *C*–*Q* behaviours.

2 | SITE DESCRIPTION

We conducted this study in the upper Hotel Gulch watershed in the Manitou Experimental Forest, Colorado, United States (Figure 1). The watershed is in a montane environment with a semi-arid climate

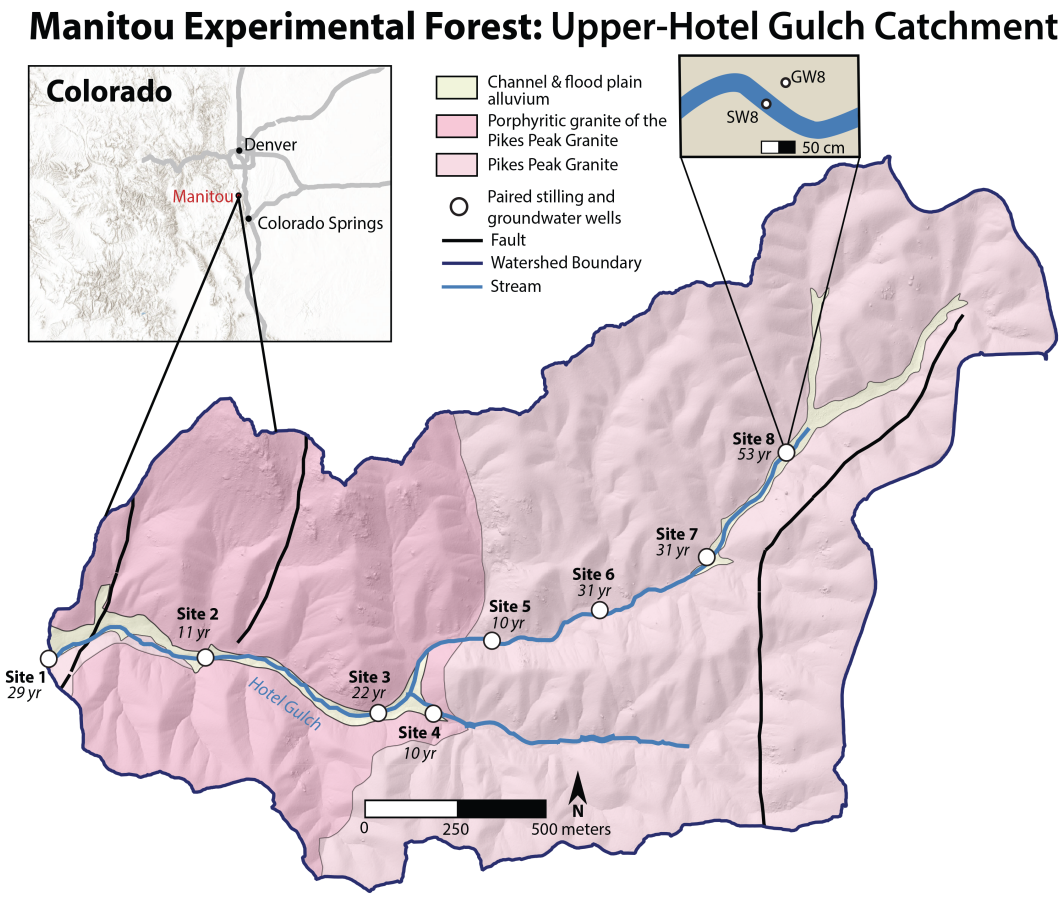

FIGURE 1 Map of the upper-Hotel Gulch catchment within the Manitou Experimental Forest, Colorado, USA. Paired stilling and groundwater wells at sites 1–8 are displayed as circles. The groundwater age in June 2021, as determined in Warix et al. (2023), is listed under each site. All groundwater wells are located on the north bank of the stream.

and mean annual temperature of 5.5°C (1999–2020) (Frank et al., 2021). Vegetation consists of pine, mixed conifers, and aspen groves. Hotel Gulch is a first-order stream with an average outlet discharge of 3.4 L/s during April–November in 2021 and 2022. The catchment is 3 km^2 and the main stem of Hotel Gulch is 2.6 km long with an elevation range of 2601–2843 m.

The catchment has a mean annual precipitation of 36 cm (1979–2021) (NADP, 2022). During winter months (October to May) the primary form of precipitation is snow. A persistent snowpack develops on north-facing slopes, while south-facing slopes have intermittent and patchy snow cover that typically melts within days of a storm event (Bush, 2022). During summer months (June to September) the primary form of precipitation is rain which typically falls during short convective afternoon thunderstorms with brief but sometimes intense periods of rainfall (Bush, 2022). Under future climate scenarios presented in Lukas et al. (2014), the central mountains of Colorado are expected to see both increases in winter precipitation and temperature, suggesting that more precipitation will be in the form of rain during early and late winter. Snow water equivalent (SWE) in late April is expected to decrease as a function of warmer temperatures causing the timing of both peak snowmelt and melt to shift earlier in the year. In summer months, precipitation is expected to decrease while temperatures are expected to increase. In Colorado River headwaters, peak runoff is expected to shift sooner from June to May and decrease in overall magnitude.

The catchment is underlain by the Pikes Peak batholith, a hornblende-bearing biotite granite. The constituent minerals include microcline (35%–50%), quartz (20%–35%), plagioclase (10%–20%), biotite (2%–7%), and hornblende (0.5%–2%) (Temple et al., 2007). Accessory minerals include zircon, apatite, magnetite, and fluorite (Temple et al., 2007; Wanty et al., 1992). The lower watershed is underlain by the porphyritic granite of the Pikes Peak batholith (Ypb) while the upper watershed is underlain by the Pikes Peak granite (Ypp) (Temple et al., 2007; Figure 1). These two members have similar mineralogy and primarily differ in crystal size. The Pikes Peak granite is a fractured system (Blair, 1976), and fractures control groundwater flow (Wanty et al., 1992). We observed highly weathered fractures at surface outcrops. The watershed has four mapped north–south trending faults that cut or approach the stream as part of the Mount Deception Fault System (Temple et al., 2007; Figure 1). Initial jointing during magma cooling enabled fractures to form, followed by compressional stresses during Laramide tectonism during the late-Cretaceous and early Tertiary period (Blair, 1976). During the Tertiary period, uplift exposed more of the Pikes Peak batholith and enabled water to weather the granite, enabling continuous weathering over the last 40 m.y., and causing today's landscape to consist of deeply weathered rocks in an evolved geomorphic landscape (Blair, 1976).

The watershed is covered by a thin layer of soils, except where bedrock is exposed at the surface. Soils range from aquolls in the riparian zone to very gravelly coarse sandy loam to gravelly coarse sandy loam on hillslopes. The maximum soil profile thickness for mapped soil units in the watershed is 1.6 m (Moore, 1992, NRCS 2023). Channel and floodplain alluvium units consist of angular to sub-rounded pebble gravel and sand and are estimated to be 0.6–1.7 m thick (Temple et al., 2007). Additional details about watershed soil and geology can be found in Warix et al. (2023).

2.1 | Building off the hydrologic framework presented in Warix et al. (2023)

In Warix et al. (2023), we assessed drivers of hydrologic resilience by comparing physical watershed properties to groundwater-surface water connection and groundwater age. Here, we build off the existing hydrologic framework to assess the relation between hydrology and geochemistry. In 2021, we instrumented eight sites with paired stilling wells and shallow groundwater piezometers within a meter of the steam (Figure 1). Paired stilling and groundwater wells were spaced approximately evenly every 400 m along the stream, with the exception of site 4, which is located on a small tributary that connects with the main stem upstream of site 3 (Figure 1). Sites are numbered by relative order from the outlet point, with site 1 being the farthest downstream location and site 8 being the uppermost sampling location. Surface water samples are referred to as SW(*n*) and groundwater samples are referred to as GW(*n*), where n is the site number. Well coordinates and elevation are presented in Table S1 of the supplemental information. Shallow groundwater piezometers ranged from 1 to 1.8 m deep and were cased with slotted 3.8-cm (1.5-inch) PVC. The bottom 80% of wells was screened to capture a mixed signal of all groundwater contributing to the stream. Stilling wells were installed in the middle of the stream channel (average stream width is approximately 50 cm) with 5.1-cm (2-inch) PVC. For complete details on well installation and screening, see Warix et al. (2023).

The Hotel Gulch stream is primarily groundwater supported year-round (Warix et al., 2023), even during storm events (Bush, 2022). 85% of hydrograph separation observations show that the groundwater fraction of streamflow is greater than 70%, based on a two end-member mixing model from Warix et al. (2023). Groundwater sourcing streamflow is stored in riparian alluvial aquifers, deeper granitic fractures, or is seasonally sourced from hillslope interflow. We observed that storage and flow mechanisms are controlled by local watershed topography. In the steepest portions of the catchment (sites 2–6), seasonally variable interflow sources streamflow, while in flatter portions of the catchment, such as at sites 7 and 8, alluvial aquifers provide shallow-subsurface storage that source old groundwater to the stream. At site 1, a fault crosses the stream, causing old water to source streamflow (Warix et al., 2023).

We determined mean groundwater age for groundwater samples collected on June 9–10 and September 24–25, 2021 using tritium and chlorofluorocarbon-12 in Warix et al. (2023). We assumed binary mixing between young and old piston flow and used TracerLPM to determine the mean age of groundwater. Groundwater age across all eight sites ranged from 10 to 53 years (Figure 1). The youngest water (10–25 years) was found in the middle catchment sites (sites 2–6) while older water (29–53 years) was found in the upper and lowermost portions of the catchment (sites 1, 7, and 8) (Figure 1). Groundwater age

typically increased from June to September, 2021 with the largest age increases occurring at sites 1, 4, 5, and 6 where local slope is highest. Sites 3, 7, and 8 had a relatively constant age in both the spring and fall. Complete mean groundwater age results can be found in Warix et al. (2023).

3 | METHODS

We combined field data observations of stream discharge and stream and groundwater chemistry to evaluate *C*–*Q* relations. We also collected whole rock and clay samples from the riparian zone for XRD analyses, with the goal of mapping the importance of clays and cation exchange on our *C*–*Q* relations. Finally, we calculated mineral saturation and created activity diagrams in Geochemist's Workbench, a geochemical modelling program.

3.1 | Field data collection

3.1.1 | Stream discharge

We measured water level in stilling wells every 15 min at all eight sites from April–November of 2021 and 2022 with Onset HOBO U-20-001 water level loggers. Eight rating curves were created from discharge measurements with the salt dilution method (Moore, 2005) to continuously estimate stream discharge. Manual discharge was collected between 25 and 29 times at each site over a two-year period. Discharge results from 2021 are also presented in Warix et al. (2023).

3.1.2 | Stream and groundwater chemistry

Surface-water and groundwater chemistry samples were collected approximately twice a month from April to November 2021 and 2022. In 2021, groundwater was not collected until June. Chemistry samples were not collected during or immediately after storm events and so the chemistry around the highest discharge events is not represented in this study. Surface-water samples were collected by hand near the stilling well before salt dilution discharge measurements. Groundwater samples were collected with Viton (2021) or silicon (2022) tubing and a peristaltic pump. Two blanks and one duplicate were collected during each sampling day. Stream and groundwater pH, specific conductivity, and temperature were determined in the field with a ThermoFisher Orion Star A329 portable multiparameter meter. In this paper we primarily focus on five major ions, Al^{3+}, Ca^{2+}, Mg^{2+}, Na^{+}, and $SiO_{2(aq)}$, which are solutes that are primarily sourced to groundwater by water-rock interactions. Additional cation (K^{+}) and anions (F^{-}, Cl^{-}, and SO_4^{2}) were analysed for a charge balance check, but we do not discuss them throughout the manuscript. Additional *C*–*Q* plots for these solutes are included in the supplemental index for reference.

All water samples were filtered to 0.2 μm with nylon filters before collection in 30-mL HDPE Nalgene bottles. Samples for anion concentrations were frozen before analysis using ion chromatography at the Colorado School of Mines. Anions include F^{-}, Cl^{-}, and SO_4^{2}. Samples for cation concentrations were acidified with nitric acid to a pH of 2 and refrigerated before analysis using inductively coupled plasma atomic emission spectroscopy (ICP-AES) at the Colorado School of Mines. Cations include Al^{3+}, Ca^{2+}, K^{+}, Mg^{2+}, Na^{+}, and $SiO_{2(aq)}$. Alkalinity was measured with a ThermoScientific Orion Star T910 auto-titrator with 0.1 N HCl.

3.1.3 | *C*–*Q* relations

To compare *C*–*Q* patterns across different solutes involved in water-rock interactions, we plotted Al^{3+}, Ca^{2+}, Mg^{2+}, Na^{+}, and $SiO_{2(aq)}$ concentrations and stream discharge in log–log space. The slope of the *C*–*Q* relation was determined using a power-law equation in the form of $C = aQ^{b}$, where a and b are constants. We define dilution as any slope < -0.2, mobilization as any slope >0.2, and chemostasis for slopes of 0 ± 0.2 (e.g., Li et al., 2017). To distinguish between varying degrees of chemostasis, we use the terms "strong-chemostasis" for slopes of 0 ± 0.1 and "weak-chemostasis" for slopes ranging from |0.101-0.2|.

3.2 | Whole rock and clay x-ray diffraction

We used x-ray diffraction (XRD) to determine clay phases present in riparian soil as well as Pikes Peak Granite for whole-rock analysis. Whole-rock samples were collected from outcrop obtained from a pilot borehole in the riparian zone near GW1 collected with a Shaw Backpack Drill. During groundwater-well installation we collected shallow soil samples 1 m below the surface. We air dried the samples before crushing whole rock and soil samples in a ball mill and sieving to a fine powder (<88 μm). We then added Millipore water to samples (water: rock ratio = 10:3) and trace (<1 g) sodium carbonate as a dispersing agent before centrifuging samples at 1000 rpm for 3 min to suspend particles <2 μm, following methods from Moore et al. (1989). We prepared oriented clay mounts on quartz slides by standard vacuum-filtration methods (Moore et al., 1989). Samples were analysed from 2° to 65° 2θ using a Panalytical X'pert Pro X-Ray Diffractometer. After initial XRD analysis, we put the quartz slides with adhered clay particles into a drying chamber with ethylene glycol in an oven at 50°C overnight and reanalyzed with the same parameters to detect swelling clay.

3.3 | Cation exchange characterization

We used a barium chloride ($BaCl_2$) soil-water extraction to determine exchangeable cations in Manitou soils. We isolated soil collected from the bottom of each of our 1–1.8-m deep wells. We combined 5 g of soil with a 0.1 M $BaCl_2$ solution in centrifuge tubes. Samples were slowly shaken on a shaker table for 2 h, then were centrifuged at

2500 rpm for 10 min following methods from Hendershot and Duquette (1986). The supernatant fluid was filtered through 0.45 μm mixed cellulose esters (HAWP) filters, acidified to a pH of 2, and cations were analysed by ICP-AES.

3.4 | Geochemical modelling

In this paper, we focus on geochemical reactions involving major primary granitic minerals, such as plagioclase and biotite, and montmorillonite clays, their secondary weathering products. Plots and tables in the results discussion include solutes involved in geochemical reactions between these minerals (Al^{3+}, Ca^{2+}, Mg^{2+}, Na^{+}, $SiO_{2(aq)}$). We include other solutes (K^{+}, Cl^{-}, SO_4^{2-}) in the supplementary information for completeness.

We determined the plagioclase composition ($Na_{0.836}Ca_{0.164}Al_{1.164}Si_{2.836}O_8$) of the Pikes Peak granite near the Manitou Experimental Forest using bulk chemical analyses from sample 605 in Wobus (1976). Mineral saturation indices were calculated in Geochemist's Workbench (GWB) Community Edition 2023 using the thermos_sit.tdat database to assess favourable geochemical reactions. To calculate mineral saturation specifically for the Pikes Peak plagioclase (17% Anorthite), we used a simple linear mixing between albite (sodium plagioclase endmember) and anorthite (calcium plagioclase endmember) equilibrium constants provided in the mentioned geochemical database. Clay-mineral saturation was calculated for montmorillonite-BCCa ($Ca_{0.17}Mg_{0.34}Al_{1.66}Si_4O_{10}(OH)_2$) and montmorillonite-BCMg ($Mg_{0.17}Mg_{0.34}Al_{1.66}Si_4O_{10}(OH)_2$). Activity diagrams were also created in GWB, where we suppressed all minerals except those observed in XRD analyses (Ca- and Mg-montmorillonite, illite, and primary granitic minerals); these minerals were used to determine what geochemical reactions are driving stream solute concentrations.

4 | RESULTS AND DISCUSSION

4.1 | Discharge and chemistry observations

Average stream discharge at all eight sites was 2 L/s and ranged from 0 to 15 L/s (Figures S1, S2). Site 1 consistently had the highest discharge (mean discharge from April to November in 2021 and 2022 = 3.4 L/s) and the tributary, site 4, consistently had the lowest mean discharge over the same timespan (0.6 L/s). At all sites, discharge was highest from April to June and decreased throughout the summer and fall with occasional increases in discharge after summer monsoon rainstorms (Figure S1, S2).

Average solute concentrations were typically higher in groundwater than surface water and relative mean concentrations decreased in the following order: Ca^{2+}, Na^{+}, $SiO_{2(aq)}$, Mg^{2+}, Al^{3+} (Figures S3, S4). Like discharge, solute concentrations varied seasonally, where concentrations were lowest from April to May, increased through early September, and then began to decrease until November when the stream froze and observations ceased. Groundwater- and surface-water-solute concentrations were similar seasonally, particularly for Na^{+}, Al^{3+}, and $SiO_{2(aq)}$. Ca^{2+} and Mg^{2+} had the largest differences between groundwater- and surface-water-solute concentrations (Figures S3, S4).

4.2 | Chemostasis observed despite variability in groundwater age

All eight sites exhibited chemostasis for solutes involved in plagioclase dissolution and subsequent clay precipitation (Al^{3+}, Ca^{2+}, Mg^{2+}, Na^{+}, $SiO_{2(aq)}$), as defined by a power-law slope ranging from −0.2 to 0.2 (Figures 2, 3). $SiO_{2(aq)}$, Na^{+}, and Al^{3+} had slopes closest to zero for all eight sites and exhibited strong chemostasis while Ca^{2+} and Mg^{2+} had the most negative slopes and exhibited weak chemostasis

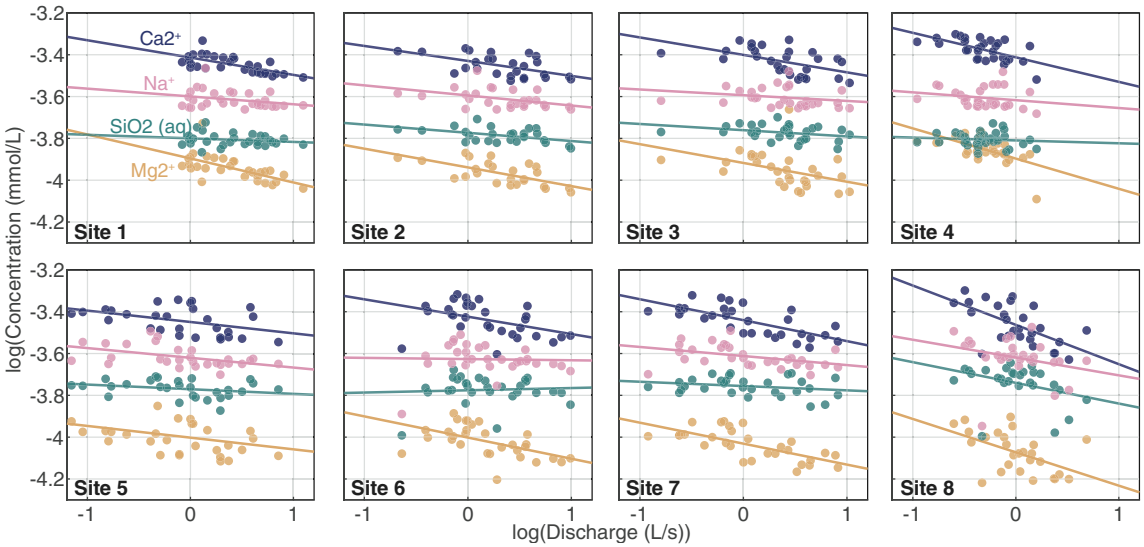

FIGURE 2 Concentration–discharge relations for Ca^{2+} (purple), Na^{+} (pink), $SiO_{2(aq)}$ (green), and Mg^{2+} (yellow) for each of the eight sites from 2021 and 2022. Data are plotted in log–log space and best fit lines are displayed for each solute in the respective colour. *C*–*Q* relations for Al^{3+} are plotted separately in Figure S5 because Al^{3+} concentrations are orders of magnitude less than solutes displayed here.

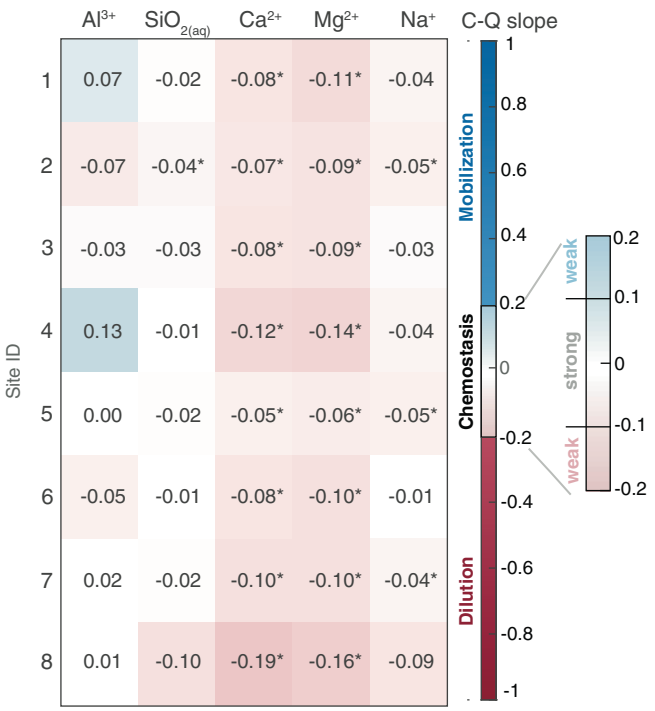

FIGURE 3 Log(C) versus log(Q) slopes (b) for five solutes, fit to equation $C = aQ^b$. Each value is coloured by slope with mobilization slopes in blue ($b > 0.2$), dilution slopes in red ($b < 0.2$), and chemostatic slopes in in shades of light blue to light pink. Al^{3+}, SiO_2(aq), and Na^+ exhibit strong chemostasis ($b \pm 0.1$) while most Ca^{2+} and Mg^{2+} slopes exhibit weak chemostasis ($b = |0.101\text{-}0.2|$). Statistically significant slopes ($p < 0.05$) are indicated with an asterisk (*).

(Figure 3). Other solutes such as Cl^-, F^-, K^+, and SO_4^{2-} also exhibited chemostasis (Figure S6, Table S2). We did not observe strong spatial trends between *C*–*Q* patterns and location in the watershed.

We compared groundwater age to *C*–*Q* slope for Al^{3+}, Ca^{2+}, Mg^{2+}, Na^+, and $SiO_{2(aq)}$ and observed no statistically significant linear relation ($p < 0.05$) for any solute (Figure 4). The lack of trend between age and *C*–*Q* slope is also observed for other solutes including K^+, Cl^-, F^-, and SO_4^{2-} (Figure S7). The large groundwater-age range (44 years) is attributed to changes in groundwater flowpath and storage mechanisms such as seasonally variable interflow, alluvial storage, and fault-sourced groundwater flow (Warix et al., 2023). The relatively consistent *C*–*Q* slopes indicate that mechanisms controlling *C*–*Q* patterns for each solute are largely independent of inferred spatiotemporal changes in streamflow source and that geochemical reactions are controlling *C*–*Q* behaviour, rather than hydrologic connection.

We also compared stream and groundwater Al^{3+}, Ca^{2+}, Mg^{2+}, Na^+, and $SiO_{2(aq)}$ concentrations collected at the same time as groundwater age samples on June 9–10 and September 24–25, 2021 to their respective groundwater age (Figure 5). Unlike other studies that have compared groundwater age to spring and stream chemistry in igneous catchments (Burns et al., 2003; Rademacher et al., 2005), we do not observe statistically significant linear trends (defined as a p-value <0.05) between age and stream- or groundwater-solute concentrations (except for groundwater $[Ca^{2+}]$ in June, 2021) (Figure 5).

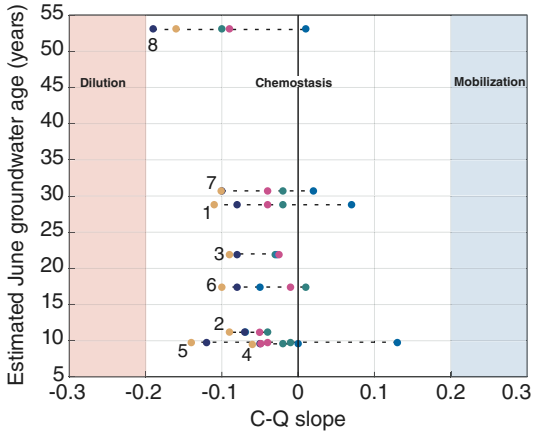

FIGURE 4 Plot comparing *C*–*Q* slope for Al^{3+} (blue), Na^+ (pink), Ca^{2+} (purple), Mg^{2+} (yellow), and $SiO_{2(aq)}$ (green) with mean groundwater age for each of the eight sites. *C*–*Q* slopes that correspond to the same site, and thus have the same groundwater age, are connected with a black dashed line and are labelled with their site number to the left of the point cluster. The white background spans from −0.2 to 0.2, the range for chemostatic slopes. Dilution and mobilization slopes are shaded in red and blue, respectively. While all *C*–*Q* slopes indicate chemostasis, no statistically significant trend between age and *C*–*Q* slope exists.

The lack of relation between groundwater age and chemistry again suggests that groundwater age, and inherently, variability in groundwater flowpaths, are not the primary drivers of stream solute concentrations and stream *C*–*Q* patterns, but rather that groundwater flowpaths are long enough to reach geochemical equilibrium, causing relatively uniform chemostasis through time and space.

We note that the age tracers used for this study (chlorofluorocarbon-12 and tritium) cannot capture variability in very young (<1 year) groundwater or soil water and we are therefore missing the comparison between the youngest component of flow and *C*–*Q* slope. However, groundwater chemistry and stream-water chemistry are similar (Figure 5, Figures S2, S3), and the stream is groundwater supported (Warix et al., 2023), suggesting that older-groundwater contributions dominate stream-water chemistry and that it is therefore reasonable to compare stream *C*–*Q* slope to shallow groundwater age as determined by CFC-12 and tritium.

4.3 | Chemostasis primarily driven by silicate mineral dissolution and clay precipitation

To investigate processes driving chemostasis at our sites, we calculated mineral saturation for the Pikes Peak plagioclase and montmorillonite and illite clays observed in XRD analyses (Figure S8). Whole-rock XRD analysis confirmed that the Pikes Peak Granite in the shallow subsurface is composed of quartz, potassium feldspar, plagioclase, and biotite, consistent with existing mineralogy descriptions (Smith et al., 1999; Temple et al., 2007; Wobus, 1976).

The Pikes Peak plagioclase ($An_{0.17}$) is approaching geochemical saturation in both groundwater and surface water (Figure 6a), while

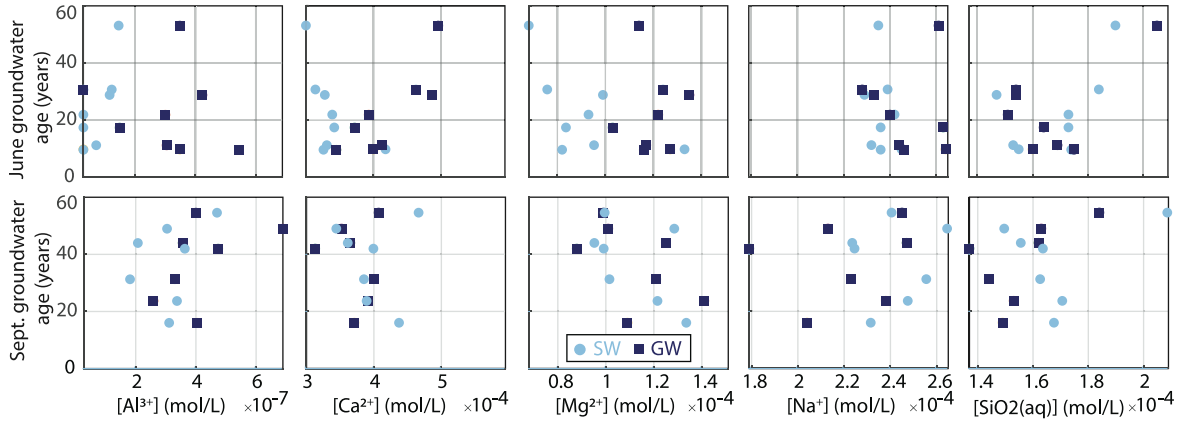

FIGURE 5 Groundwater age versus stream and groundwater chemistry collected on the same date either on June 9–10 or September 24–25, 2021 for both surface water (light blue circles) and groundwater (dark purple squares). The only statistically significant linear relation (defined as a *p*-value <0.05) is June groundwater age and calcium concentrations in groundwater.

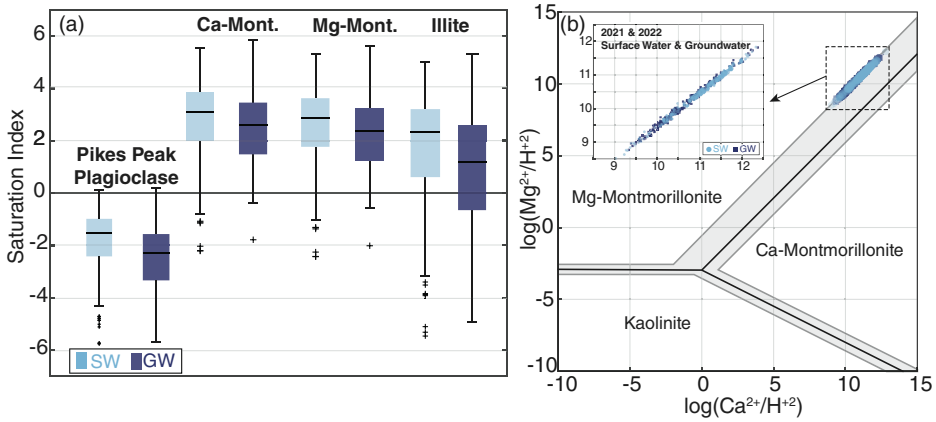

FIGURE 6 (a) Boxplots showing differences between geochemical saturation states of the Pikes Peak plagioclase, Ca-montmorillonite, Mg-montmorillonite, and illite for all surface-water and groundwater samples collected in 2021 and 2022. Negative values indicate undersaturation where the mineral is favoured to dissolve, zero indicates equilibrium, and positive values indicate that the mineral is geochemically supersaturated or favoured to precipitate. (b) All surface water and groundwater from 2021 and 2022 plot parallel to, though slightly offset from, the equilibrium line between Mg-montmorillonite and Ca-montmorillonite $\log[(Ca^{2+}/H^{+2})]$ $\log[(Mg^{2+}/H^{+2})]$ activity space, indicating equilibrium between the two minerals is a controlling process on Ca and Mg concentrations. Black lines of equilibrium on this diagram define aqueous conditions where a reaction between two phases is in geochemical equilibrium; the light-grey-shaded area represents the equilibrium constant, $\log(K_{eq})$, error within 0.2 orders of magnitude, consistent with conservative error estimates for montmorillonite clays provided in (Kittrick, 1971). Our data plot parallel to the solid line and within the expected error range indicating that the cation exchange reaction between clays is an important process, despite uncertainty in exact clay mineralogy and thermodynamic data.

secondary Ca- and Mg-montmorillonite and illite clays are geochemically saturated (Figure 6a). For Ca- and Mg-montmorillonite and illite, surface water was typically more geochemically saturated than groundwater, and Ca-montmorillonite was more geochemically saturated than Mg-montmorillonite (Figure 6a).

As described earlier, primary silicate mineral dissolution releases solutes into solution that drive clay precipitation, and clay precipitation is often slow enough to limit primary silicate dissolution by maintaining slight geochemically undersaturated conditions for primary minerals while also sustaining geochemical oversaturation of the clay phases (Maher et al., 2009). This is what we observe in Hotel Gulch (Figure 6a). We evaluated the potential for clay precipitation to influence cation concentrations with a mineral stability diagram for Ca- and Mg-containing montmorillonite clay phases (Figure 6b). Solute concentration ratios from water samples in the stream and groundwater plot parallel to, and within error, of the line of equilibrium between Mg- and Ca- montmorillonite clays, thus indicating that the stream and groundwater compositions are in equilibrium with this reaction, and that montmorillonite precipitation likely buffers Ca^{2+} and Mg^{2+} concentrations in both stream and groundwater. We postulate a set of unidirectional chemical reactions whose relative reaction rates and thermodynamic solubility constants control the $SiO_{2(aq)}$ and Al^{3+} concentrations in groundwater through dissolution of primary silicate minerals and subsequent clay precipitation:

Plagioclase dissolution:

$$Na_{0.836}Ca_{0.164}Al_{1.164}Si_{2.836}O_8 + 4.656H^+ + 3.344\,H_2O \rightarrow +1.164Al^{3+} + 0.164Ca^{2+} + 0.836Na^+ + 2.836\,H_4SiO_4.$$

Biotite dissolution:

$$KMg_3(AlSi_3O_{10})(OH)_2 + 10H^+ \rightarrow 3Mg^{2+} + K^+ + Al^{3+} + 3H_4SiO_4.$$

Ca-montmorillonite precipitation:

$$0.17Ca^{2+} + 0.34Mg^{2+} + 1.66Al^{3+} + 4H_4SiO_4 \rightarrow Ca_{0.17}Mg_{0.34}Al_{1.66}Si_4O_{10}(OH)_2 + 6H^+ + 4H_2O.$$

Mg-montmorillonite precipitation:

$$0.51Mg^{2+} + 1.66Al^{3+} + 4H_4SiO_4 \rightarrow Mg_{0.17}Mg_{0.34}Al_{1.66}Si_4O_{10}(OH)_2 + 6H^+ + 4H_2O.$$

We propose that these dissolution and precipitation reactions drive a steady-state balance in groundwater-cation concentrations as groundwater flows through the fractured rock, and dissolves cations in streamflow that are involved in downgradient reactions. Because the stream is primarily groundwater supported, even during high-flow events, changes in stream discharge do not influence cation concentrations because source water is at geochemical equilibrium. For Al^{3+} and $SiO_{2(aq)}$, most *C*–*Q* behaviour is characterized by slopes between 0±0.1, indicating strong chemostasis, while Mg^{2+} and Ca^{2+} exhibit weak chemostasis with a range of −0.05 to −0.19 and an average slope of −0.102 (Table 1). Our conclusion that old, geochemically-evolved water undergoing clay precipitation is the dominant driver of chemostasis is consistent with findings from Maher (2010), who suggest that in a transport-limited system with groundwater age greater than 10 years, weathering is thermodynamically controlled. Our results corroborate the modelling-informed conclusion that systems with old-groundwater supported streams are chemostatic (Maher, 2011) as all our sites exhibited chemostasis, were at least 10 years old (Figure 1), and had an old component to flow (Warix et al., 2023).

4.4 | Cation exchange as a secondary control on Mg^{2+} and Ca^{2+}

Cation concentrations from the exchangeable sites of soil samples at each of the eight sites are presented in Table 1. The cation-exchange pool consists of solutes that can be exchanged on montmorillonite clay surfaces. In Manitou soils, Ca^{2+} made up 73%–83% of the calcium + magnesium + potassium + sodium exchange pool at all sites, followed by 12%–18% Mg^{2+}, 3%–9% K^+, and 1%–4% Na^+, indicating that divalent cations make up the majority of exchangeable cations. We did not observe strong spatial trends between exchangeable cations and location of soil in the watershed.

We explore the potential that cation exchange exerts as an additional control on Ca^{2+} and Mg^{2+} *C*–*Q* behaviour, causing the slightly lower *C*–*Q* slopes for these solutes compared to Al^{3+} and $SiO_{2(aq)}$. The soil cation-exchange pool of riparian sediments at Manitou is dominated by Ca^{2+} and Mg^{2+}, comprising an average 78% and 15% of the exchange pool, respectively.

Stream Ca/Mg ratios decreased downstream, except for the tributary at site 4 as indicated by the light-blue boxplots in Figure 7. Groundwater Ca/Mg ratios also decreased downstream, but with some variability. Groundwater and surface water Ca/Mg ratios that are significantly different from one another (two-tailed *t*-test *p*-value <0.05) are indicated with an asterisk (Figure 7). While not perfectly linear, we observed a similar longitudinal decrease in Ca/Mg ratios in cations extracted from riparian soils moving from Site 8 to Site 1 (Table 1), providing additional evidence of cation exchange impacting stream and soil chemistry along longitudinal flowpaths. The longitudinal decrease in Ca/Mg along the stream is likely due to rapid exchange of calcium with clays increasingly enriched in magnesium in the shallow soil zone. We hypothesize that longitudinally shifting ratios are due to heterogeneity in the relative ratio of primarily Ca- to Mg-montmorillonite clays, which was not detectable with the clay XRD methods we used. Shifting ratios as a result of changing mineralogy is consistent with expectations for a system with cation exchange because of fast reactions that buffer changes in stream solute concentrations.

The relatively fast cation-exchange reactions, compared to timescales for clay precipitation, make Ca^{2+} and Mg^{2+} concentrations

TABLE 1 Cation concentrations and ratios in riparian Manitou soils.

Sample ID	Ca (mmol/kg)	Mg	K	Na	Si	Ca/Mg	Mg/Na (-)	Ca/Na
Site 1	25.1	5	1.4	1.3	0.2	5.0	19.9	4.0
Site 2	39.6	7.8	2.4	0.9	0.3	5.1	45.5	9.0
Site 3	41.7	7.4	2.5	1.1	0.3	5.7	36.9	6.5
Site 4	35.4	8.2	1.6	0.8	0.2	4.3	45.2	10.5
Site 5	34.9	7.7	2.3	1.0	0.2	4.5	34.9	7.7
Site 6	25.6	5.6	3	0.9	0.2	4.5	28.1	6.2
Site 7	84.2	13.3	3.1	1.2	0.4	6.4	69.1	10.9
Site 8	43.6	6.6	3.1	1.0	0.2	6.6	45.6	6.9

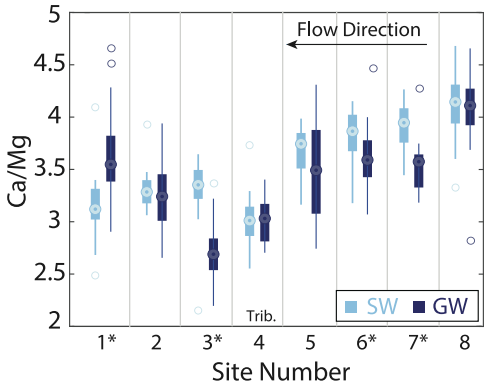

FIGURE 7 Boxplots showing Ca/Mg (mole ratio) in surface water (light blue) and groundwater (dark purple). Sites with significantly different Ca/Mg values between groundwater and surface water, as determined by a two-tailed t-test at the 0.05 significance level, have an asterisk next to the site number label (Sites 1, 3, 6, and 7). In surface water, Ca/Mg decreases downstream. Ca/Mg in groundwater and soils also decreases downstream, with some variability. Site 4 is a tributary and is not along the main-stem stream, as indicated by the "Trib." label above Site 4 label.

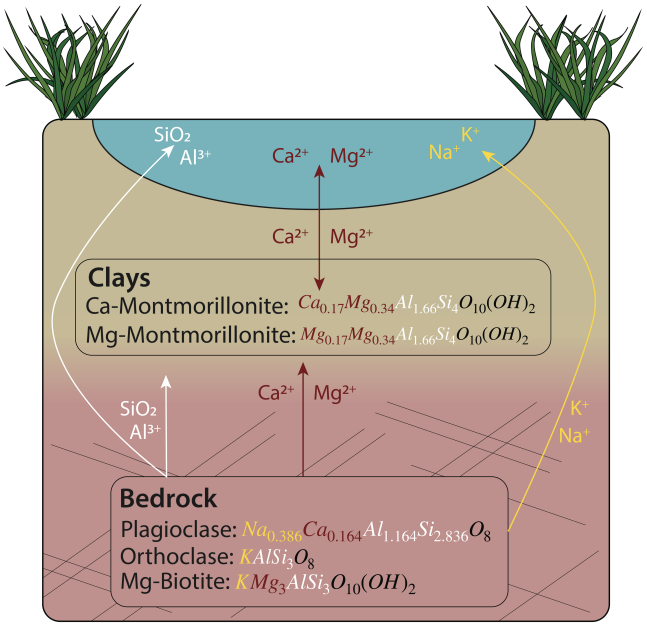

FIGURE 8 Conceptual diagram illustrating geochemical fluxes and controls driving stream concentration-discharge patterns at Manitou. White arrows indicate reactions involving the dissolution of primary granitic minerals into dissolved Al^{3+} and $SiO_{2(aq)}$ or precipitated into secondary clays. Red arrows indicate cation exchange reactions between bedrock minerals and clays, as well as clays and the stream. Yellow arrows indicate dissolution of K^+ and Na^+ from bedrock into streamflow. We note that K^+ can also be taken up by vegetation, but do not discuss it in the water-rock interaction context of this study.

more susceptible to changes associated with discharge, which we propose as the cause of slightly lower, but still chemostatic, *C*–*Q* slopes of these divalent cations compared to Al^{3+} and $SiO_{2(aq)}$. This weak chemostasis for divalent cations, relative to Al^{3+} and $SiO_{2(aq)}$, has been observed in other catchments (Conroy et al., 2022; Godsey et al., 2009, 2019; Herndon et al., 2015; Kim et al., 2017) but is rarely attributed to cation exchange.

4.5 | Coupled geochemical reactions drive chemostasis, rather than hydrologic variability

Despite a 44-year range in groundwater age and groundwater source, all solutes and sites exhibit chemostasis, leading to the conclusion that *C*–*Q* patterns are not sensitive to changes in the way that groundwater is stored and transported through the subsurface before contributing to streamflow. Warix et al. (2023) show three distinct flowpaths that source streamflow: 1) relatively young interflow that primarily occurs in steep areas during the spring; 2) shallow alluvial storage where alluvial fill is present that sources the stream year-round with relatively old groundwater; and 3) deep, older groundwater stored in granite fractures that is the primary stream source during low-flow periods. All of these flowpaths enable groundwater flow to dissolve and approach saturation with respect to granitic minerals such as plagioclase, feldspar, and Mg-biotite, causing secondary clay precipitation to occur. This clay precipitation enables subsequent cation exchange in exchangeable cation sites in Ca- and Mg-montmorillonite (Figure 8). At Manitou, mean groundwater age is long enough to reach mineral saturation, causing primary mineral dissolution and clay precipitation to be the primary driver of chemostasis. Cation exchange in riparian clays is a secondary control on stream *C*–*Q* patterns for base cations.

Rather than hydrologic variability driving changes in stream concentrations, as implied by the inherent nature of a *C*–*Q* plot with the independent (discharge) and dependent (concentration) axes, stream-solute concentrations at this site are driven by subsurface geochemical reactions. Results from this and other similar studies, although in catchments with notably different geology (e.g., Hoagland et al., 2017; Li et al., 2017), suggest that geogenic *C*–*Q* patterns can be primarily driven by geochemical reactions, rather than variability in surface flows. We also present evidence that rapid cation exchange is a secondary control on divalent-cation *C*–*Q* behaviour in this granitic montane catchment and because of this conclusion, we hypothesize that cation exchange is also similarly influencing stream Ca^{2+} and Mg^{2+} solute concentrations in other watersheds where clays exist near the stream. We show that when using *C*–*Q* as a tool to investigate streamflow source, it is important to identify geochemical reactions driving stream-solute concentrations as these reactions may drive chemostasis. When predicting future *C*–*Q* patterns and stream health and resilience, we need to consider both physical changes in hydrology and the geochemical reactions that drive solute concentrations.

This study was conducted in a small headwater catchment, but the findings should be transferrable to larger systems with groundwater-supported streams. We show that chemostasis is driven by groundwater at geochemical equilibrium, rather than changes in stream discharge. In larger systems where streams are also supported

by groundwater, we expect that chemostasis will still occur where groundwater residence times are long enough for geochemical equilibrium to occur. Our findings may not be transferrable to a catchment with distinct geologic differences in a watershed. For example, in a hypothetical catchment with headwater reaches that are underlain by granite and an outlet underlain by carbonates, geochemical reactions will shift longitudinally. The hypothetical system would transition from dissolving igneous bedrock and precipitating silicate clays in the upper catchment, to dissolving carbonate rocks and precipitating secondary carbonate minerals in the lower catchment. These changing reactions could cause an initial shift away from geochemical equilibrium and chemostasis, even where streams are consistently groundwater supported. The conclusions of this paper are still relevant to more geologically heterogeneous systems; however, as geochemical reactions are still the primary driver of *C*–*Q* response and are a function of watershed geology in groundwater-supported systems.

4.6 | Implications for solute export and chemostasis in a future warmer climate

Hydrologists have begun to observe and model how groundwater flow may shift in response to changing recharge patterns and flowpaths because of climate change. However, where chemostasis is observed, stream-solute concentrations are inherently insensitive to changes in discharge, thus indicating that solute concentrations are not driven by hydrologic variability. Therefore, potential future changes in stream-solute concentrations and *C*–*Q* behaviour are likely to be driven by subsurface geochemical reactions.

At Manitou, as well as throughout Colorado River headwaters in the western United States, future increases in temperature are expected to cause a transition from more snow- to rain-dominated systems, potentially shifting the timing of peak melt earlier in the year. While these changes will have impacts on total recharge and the way that groundwater is stored and transported in the subsurface (Meixner et al., 2016), we do not expect parallel shifts in *C*–*Q* slope because the geochemical reactions that shape groundwater chemistry will remain the same. One potential exception is if decreases in recharge are so substantive that the groundwater table elevation decreases enough to change the air-groundwater table interface, altering the types of geochemical reactions that are occurring in the subsurface. Our primary conclusion remains the same, however, because geochemical reactions are shaping *C*–*Q*.

The old landscape age of the Manitou watershed enables a transport-limited groundwater system, as 40 Ma of Pikes Peak granite weathering (Blair, 1976) has established preferential flowpaths along fractures in the granite. In fractured-igneous systems, weathering rates scale and slow through time as reaction fronts propagate and lead to zones of low reactivity, as observed and modelled in Gordon Gulch, a small headwater catchment with similar climate and geology (Andrews et al., 2023). In a fractured-granite system such as at Manitou, these low-reactivity fractures coupled with long groundwater residence times enable clays to become geochemically saturated and drive stream chemostasis for solutes involved in both primary mineral dissolution and secondary mineral precipitation, notability $SiO_{2(aq)}$ and Al^{3+}. We therefore predict that where decreases in recharge cause water to move more slowly through existing flowpaths, *C*–*Q* patterns will not differ significantly as the system is already at geochemical equilibrium and because we observed the same geochemical controls throughout the watershed despite variability in groundwater flowpaths and groundwater age.

We also show that cation exchange in riparian clays is a secondary control on stream chemostasis for base cations. Stream and groundwater Ca/Mg were relatively constant through space, relative to observed variability in soil Ca/Mg, indicating an abundant pool of exchangeable cations (Figure 3, 7, Table 1). We suggest that cation exchange will continue to drive weak chemostasis for base cations if clays are present in the riparian zone, which are not expected to change in future climate scenarios. This conclusion that where clays are not present, *C*–*Q* slopes will be closer to zero is consistent with models in Li et al. (2017) who show that increasing cation exchange capacity in riparian soils causes *C*–*Q* slope to shift from strong to weak chemostasis.

As watershed aridity increases in many systems due to climate change, reaction rates have been hypothesized to increase, leading to higher mean stream-solute concentrations (Li et al., 2022). Stream-solute concentrations have been observed to increase over the last 30 years in catchments throughout the United States (Heil et al., 2022; Li et al., 2022). However, despite these increases in solute concentrations, we do not expect a proportional change in *C*–*Q* slope as increasing solute concentrations (C) will be buffered by decreases in stream discharge (*Q*) as a result of increasing aridity. While we do not present a multi-decadal timeseries, space-for-time substitution to make predictions about future *C*-*Q* behavior. The lack of relation between *C*–*Q* slope, groundwater age, and streamflow source through space suggests that stream *C*–*Q* patterns in systems such as Manitou are not sensitive to future changes in stream discharge where the system is already at geochemical equilibrium.

5 | CONCLUSIONS

We combined 2 years of *C*–*Q* data with groundwater-age estimates at eight locations along a granitic montane headwater stream to identify drivers of chemostasis and suggest how climate change may impact future stream *C*–*Q* patterns. Unlike many hydrology studies that characterize *C*–*Q* patterns, we identified which geochemical reactions shape groundwater chemistry before contributing to streamflow. We show that in chemostatic systems, stream *C*–*Q* slopes are independent of groundwater age for solutes involved in water-rock interactions because groundwater is sufficiently old enough to reach geochemical equilibrium. Long groundwater residence times enable sufficient time for primary mineral dissolution and subsequent clay precipitation reactions to occur. These reactions drive strong chemostasis for Al^{3+} and $SiO_{2(aq)}$. However, in the shallow soil zone, clays that are formed as a result of granite dissolution enable cation

exchange which buffers base-cation concentrations, causing weak chemostasis for Ca^{2+} and Mg^{2+}. We suggest that cation exchange as a *C–Q* control is largely ignored because of a disconnect between hydrologists and geochemists, and that collaboration between hydrologists and geochemists can identify how geochemical reactions change along a flowpath to more fully delineate *C–Q* controls. As a result of the conclusion that that chemostasis is primarily controlled by geochemical reactions, rather than by changes in hydrology, we predict that where recharge patterns shift and alter flowpaths, stream *C–Q* slope will remain constant because mechanisms controlling stream chemistry are independent to decreases in surface flows.

ACKNOWLEDGMENTS

We thank Samantha Motz, Sadie Jonson, Shradhanjli Ravikumar, and Luke Jacobsen for field assistance. In addition, we thank Holly Barnard and Sidney Bush for helpful discussions. Finally, we thank Steven Alton and Paula Fornwalt for Manitou Experimental Forest management. This work is supported by the National Science Foundation under Award No. EAR-2012730. Additional funding was provided by the Geological Society of America Graduate Student Research Grants program.

DATA AVAILABILITY STATEMENT

Concentration-discharge, soil extraction, and XRD data are available at https://www.hydroshare.org/resource/c4b384a77a0f43cbb2de2d6eae9cf901/.

REFERENCES

Andrews, E., & Navarre-Sitchler, A. (2021). Temporal and spatial heterogeneity of mineral dissolution rates in fractured media. *Geochimica et Cosmochimica Acta*, *312*, 124–138. https://doi.org/10.1016/j.gca.2021.08.008

Andrews, E. M., Hyman, J. D., Sweeney, M. R., Karra, S., Moulton, J. D., & Navarre-Sitchler, A. (2023). Fracture intensity impacts on reaction front propagation and mineral weathering in three-dimensional fractured media. *Water Resources Research*, *59*, 1–20. https://doi.org/10.1029/2022WR032121

Beisner, K. R., Solder, J. E., Tillman, F. D., Anderson, J. R., & Antweiler, R. C. (2020). Geochemical characterization of groundwater evolution south of grand canyon, Arizona (USA). *Hydrogeology Journal*, *28*, 1615–1633. https://doi.org/10.1007/s10040-020-02192-0

Blair, R. W. (1976). Weathering and geomorphology of the Pikes Peak granite in the southern rampart range, Colorado. In *Professional contributions of Colorado School of Mines: Studies in Colorado, Field Geology* (pp. 68–72). Colorado School of Mines Press.

Burns, D. A., Plummer, L. N., McDonnell, J. J., Busenberg, E., Casile, G. C., Kendall, C., Hooper, R. P., Freer, J. E., Peters, N. E., Beven, K., & Schlosser, P. (2003). The geochemical evolution of riparian groundwater in a forested piedmont catchment. *Groundwater*, *41*, 913–925. https://doi.org/10.1111/j.1745-6584.2003.tb02434.x

Bush, S. A. (2022). *Ecohydrologic processes in the montane headwaters of the upper South Platte River*. University of Colorado Boulder.

Capuano, R. M., & Jones, C. R. (2020). Cation exchange in groundwater-chemical evolution and prediction of paleo-groundwater flow: A natural-system study. *Water Resources Research*, *56*, 1–22. https://doi.org/10.1029/2019WR026318

Carroll, R. W. H., Manning, A. H., Niswonger, R., Marchetti, D., & Williams, K. H. (2020). Baseflow age distributions and depth of active groundwater flow in a snow-Dominated Mountain Headwater Basin. *Water Resources Research*, *56*, 1–19. https://doi.org/10.1029/2020WR028161

Chorover, J., Derry, L. A., & McDowell, W. H. (2017). Concentration-discharge relations in the critical zone: Implications for resolving critical zone structure, function, and evolution. *Water Resources Research*, *53*, 8654–8659. https://doi.org/10.1002/2017WR021111

Clow, D. W., & Mast, M. A. (2010). Mechanisms for chemostatic behavior in catchments: Implications for CO_2 consumption by mineral weathering. *Chemical Geology*, *269*, 40–51. https://doi.org/10.1016/j.chemgeo.2009.09.014

Conroy, N. A., Dann, J. B., Newman, B. D., Heikoop, J. M., Arendt, C., Busey, B., et al. (2022). Chemostatic concentration–discharge behaviour observed in a headwater catchment underlain with discontinuous permafrost. *Hydrological Processes*, *36*(5), 1–11.

Datry, T., Arscott, D. B., & Sabater, S. (2011). Recent perspectives on temporary river ecology. *Aquatic Sciences*, *73*, 453–457. https://doi.org/10.1007/s00027-011-0236-1

Drever, J. I. (1998). *The geochemistry of natural waters: Surface and groundwater environments* (Third ed.). Prentice Hall.

Eeman, S., De Louw, P. G. B., & van der Zee, S. E. A. T. M. (2017). Cation exchange in a temporally fluctuating thin freshwater lens on top of saline groundwater. *Hydrogeology Journal*, *25*, 223–241. https://doi.org/10.1007/s10040-016-1475-y

Evans, C., & Davies, T. D. (1998). Causes of concentration/discharge hysteresis and its potential as a tool for analysis of episode hydrochemistry. *Water Resources Research*, *34*, 129–137. https://doi.org/10.1029/97WR01881

Fang, Z., Carroll, R. W. H., Schumer, R., Harman, C., Wilusz, D., & Williams, K. H. (2019). Streamflow partitioning and transit time distribution in snow-dominated basins as a function of climate. *Journal of Hydrology*, *570*, 726–738. https://doi.org/10.1016/j.jhydrol.2019.01.029

Frank, J. M., Fornwalt, P. J., Asherin, L. A., & Alton, S. K. (2021). *Manitou experimental forest hourly meteorology data* (3rd ed.). Forest Service Research Data Archive.

Genereux, D. P., Webb, M., & Kip Solomon, D. (2009). Chemical and isotopic signature of old groundwater and magmatic solutes in a costa Rican rain forest: Evidence from carbon, helium, and chlorine. *Water Resources Research*, *45*, 1–14. https://doi.org/10.1029/2008WR007630

Godsey, S. E., Kirchner, J. W., & Clow, D. W. (2009). Concentration-discharge relationships reflect chemostatic characteristics of US catchments. *Hydrological Processes*, *23*, 1844–1864. https://doi.org/10.1002/hyp.7315

Godsey, S. E., Hartmann, J., & Kirchner, J. W. (2019). Catchment chemostasis revisited: Water quality responds differently to variations in weather and climate. *Hydrological Processes*, *33*(24), 3056–3069.

Gooseff, M. N., McKnight, D. M., & Runkel, R. L. (2004). Reach-scale cation exchange controls on major ion chemistry of an Antarctic glacial meltwater stream. *Aquatic Geochemistry*, *10*, 221–238. https://doi.org/10.1007/s10498-004-2260-4

Heil, E., Warix, S., & Singha, K. (2022). Decadal trends in solute concentrations, mass flux, and discharge reveal variable hydrologic and geochemical response to climate change in two alpine watersheds. *Applied Geochemistry*, *144*, 105402. https://doi.org/10.1016/j.apgeochem.2022.105402

Hendershot, W. H., & Duquette, M. (1986). A simple barium chloride method for determining cation exchange capacity and exchangeable cations. *Soil Science Society of America Journal*, *50*, 605–608. https://doi.org/10.2136/sssaj1986.03615995005000030013x

Herndon, E. M., Dere, A. L., Sullivan, P. L., Norris, D., Reynolds, B., & Brantley, S. L. (2015). Landscape heterogeneity drives contrasting concentration-discharge relationships in shale headwater catchments.

Hydrology and Earth System Sciences, *19*, 3333–3347. https://doi.org/10.5194/hess-19-3333-2015

Hoagland, B., Russo, T. A., Xin, G., Hill, L., Kaye, J., Forsythe, B., & Brantley, S. L. (2017). Hyporheic zone influences on concentration-discharge relationships in a headwater sandstone stream. *Water Resources Research*, *53*, 4643–4667. https://doi.org/10.1002/2016WR019717.Received

Hotovy, O., Nedelcev, O., & Jenicek, M. (2023). Changes in rain-on-snow events in mountain catchments in the rain–snow transition zone. *Hydrological Sciences Journal*, *68*, 1–13. https://doi.org/10.1080/02626667.2023.2177544

Johnson, N. M., Likens, G. E., Bormann, F. H., Fisher, D. W., & Pierce, R. S. (1969). A working model for the variation in stream water chemistry at the Hubbard brook experimental Forest. *New Hampshire Water Resource Research*, *5*, 1353–1363. https://doi.org/10.1029/WR005i006p01353

Kim, H., Dietrich, W. E., Thurnhoffer, B. M., Bishop, J. K. B., & Fung, I. Y. (2017). Controls on solute concentration-discharge relationships revealed by simultaneous hydrochemistry observations of hillslope runoff and stream flow: The importance of critical zone structure. *Water Resources Research*, *53*, 1424–1443. https://doi.org/10.1002/2016WR019722

Kittrick, J. A. (1971). Montmorillonite equilibria and the weathering environment. *Proceedings of the Soil Science Society of America*, *35*, 815–820. https://doi.org/10.2136/sssaj1971.03615995003500050049x

Klos, Z. P., Link, T. E., & Abatzoglou, J. T. (2014). Extent of the rain-snow transition zone in the western U.S. under historic and projected climate. *Geophysical Research Letters*, *41*(13), 4560–4568. https://doi.org/10.1002/2014GL060500

Knapp, J. L. A., Li, L., & Musolff, A. (2022). Hydrologic connectivity and source heterogeneity control concentration–discharge relationships. *Hydrological Processes*, *36*, 1–16. https://doi.org/10.1002/hyp.14683

Langmuir, D. (1997). *Aqueous environmental geochemistry*. Prentice-Hall.

Li, L., Bao, C., Sullivan, P. L., Brantley, S. L., Shi, Y., & Duffy, C. (2017). Understanding watershed hydrogeochemistry: 2. Synchronized hydrological and geochemical processses drive stream chemostatic behavior. *Water Resources Research*, *53*(3), 2346–2367. https://doi.org/10.1002/2016WR018935

Li, L., Stewart, B., Zhi, W., Sadayappan, K., Ramesh, S., Kerins, D., Sterle, G., Harpold, A., & Perdrial, J. (2022). Climate controls on river chemistry. *Earth's Future*, *10*, 1–17. https://doi.org/10.1029/2021EF002603

Lukas, J., Barsugli, J., Doeksen, N., Rangwala, I., & Wolter, K. (2014). *Climate change in Colorado* (pp. 1–108). University of Colorado Boulder.

Maher, K. (2010). The dependence of chemical weathering rates on fluid residence time. *Earth and Planetary Science Letters*, *294*, 101–110. https://doi.org/10.1016/j.epsl.2010.03.010

Maher, K. (2011). The role of fluid residence time and topographic scales in determining chemical fluxes from landscapes. *Earth and Planetary Science Letters*, *312*, 48–58. https://doi.org/10.1016/j.epsl.2011.09.040

Maher, K., Steefel, C. I., DePaolo, D. J., & Viani, B. E. (2006). The mineral dissolution rate conundrum: Insights from reactive transport modeling of U isotopes and pore fluid chemistry in marine sediments. *Geochimica et Cosmochimica Acta*, *70*, 337–363. https://doi.org/10.1016/j.gca.2005.09.001

Maher, K., Steefel, C. I., White, A. F., & Stonestrom, D. A. (2009). The role of reaction affinity and secondary minerals in regulating chemical weathering rates at the Santa Cruz soil Chronosequence, California. *Geochimica et Cosmochimica Acta*, *73*, 2804–2831. https://doi.org/10.1016/j.gca.2009.01.030

Malcolm, R. L., & Kennedy, V. C. (1969). Rate of cation exchange on clay minerals as determined by specific-ion electrode techniques. *Soil Science Society of America Journal*, *33*, 247–253. https://doi.org/10.2136/sssaj1969.03615995003300020024x

Manning, A. H., Clark, J. F., Diaz, S. H., Rademacher, L. K., Earman, S., & Niel Plummer, L. (2012). Evolution of groundwater age in a mountain watershed over a period of thirteen years. *Journal of Hydrology*, *460–461*, 13–28. https://doi.org/10.1016/j.jhydrol.2012.06.030

Meixner, T., Manning, A. H., Stonestrom, D. A., Allen, D. M., Ajami, H., Blasch, K. W., Brookfield, A. E., Castro, C. L., Clark, J. F., Gochis, D. J., Flint, A. L., Neff, K. L., Niraula, R., Rodell, M., Scanlon, B. R., Singha, K., & Walvoord, M. A. (2016). Implications of projected climate change for groundwater recharge in the western United States. *Journal of Hydrology*, *534*, 124–138. https://doi.org/10.1016/j.jhydrol.2015.12.027

Moore, D. M., Reynolds, R. C., & Reynolds, R. C. (1989). *X-ray diffraction and the identification and analysis of clay minerals*. Oxford University Press.

Moore, R. (1992). *Soil survey of Pike National Forest, Eastern Park, Colorado, parts of Douglas, El Paso, Jefferson, and Teller counties*. USDA Forest Service and Soil Conservation Services.

Moore, R. D. D. (2005). Slug injection using salt in solution. Streamline. *Watershed Management Bullettin*, *8*, 1–6.

National Atmospheric Deposition Program. (2022). *National atmospheric deposition program (NRSP-3)* (Vol. 465). NADP Program Office, Wisconsin State Laboratory of Hygiene.

Rademacher, L. K., Clark, J. F., Clow, D. W., & Hudson, G. B. (2005). Old groundwater influence on stream hydrochemistry and catchment response times in a small Sierra Nevada catchment: Sagehen Creek, California. *Water Resources Research*, *41*, 1–10. https://doi.org/10.1029/2003WR002805

Rademacher, L. K., Clark, J. F., Hudson, G. B., Erman, D. C., & Erman, N. A. (2001). Chemical evolution of shallow groundwater as recorded by springs, Sagehen basin; Nevada County, California. *Chemical Geology*, *179*, 37–51. https://doi.org/10.1016/S0009-2541(01)00314-X

Segura, C. (2021). Snow drought reduces water transit times in headwater streams. *Hydrological Processes*, *35*, 1–17. https://doi.org/10.1002/hyp.14437

Smith, D. R., Noblett, J., Wobus, R. A., Unruh, D., Douglass, J., Beane, R., Davis, C., Goldman, S., Kay, G., Gustavson, B., Saltoun, B., & Stewart, J. (1999). Petrology and geochemistry of late-stage intrusions of the A-type, mid-Proterozoic Pikes Peak batholith (Central Colorado, USA): Implications for petrogenetic models. *Precambrian Research*, *98*, 271–305. https://doi.org/10.1016/S0301-9268(99)00049-2

Soil Survey Staff, Natural Resources Conservation Service (NRCS), & United States Department of Agriculture. (2023). Web soil survey. Retrieved from http://websoilsurvey.sc.egov.usda.gov/

Temple, J., Madole, R., Keller, J. W., Martin, D., & Woodland Park, C. O. (2007). Geologic map of the Mount Deception quadrangle, Teller and El Paso counties, Colorado. *Geological Survey Open-File Report*, OF-07-07.

Torres, M., Joshua West, A., & Clark, K. E. (2015). Geomorphic regime modulates hydrologic control of chemical weathering in the Andes-Amazon. *Geochimica et Cosmochimica Acta*, *166*, 105–128. https://doi.org/10.1016/j.gca.2015.06.007

Wanty, R. B., Folger, P. F., Frishman, D., Briggs, P. H., Day, W. C., & Poeter, E. (1992). *Weathering of Pikes Peak granite: Field, experimental, and modelling observations*. Water-Rock Interaction.

Warix, S. R., Navarre-Sitchler, A., Manning, A. H., & Singha, K. (2023). Local topography and streambed hydraulic conductivity influence riparian groundwater age and groundwater-surface water connection. *Water Resources Research*, *59*, 1–22. https://doi.org/10.1029/2023WR035044

Winnick, M. J., & Maher, K. (2018). Relationships between CO_2, thermodynamic limits on silicate weathering, and the strength of the silicate weathering feedback. *Earth and Planetary Science Letters*, *485*, 111–120. https://doi.org/10.1016/j.epsl.2018.01.005

Wobus, R. A. (1976). New data on potassic and sodic plutons of the Pikes Peak batholith, Central Colorado. In R. C. Epis & R. J. Weimer (Eds.), *Professional contributions of Colorado Schoool of Mines: Studies in Colorado field geology number 8* (pp. 57–67). Colorado School of Mines Press.

Wondzell, S. M. (2011). The role of the hyporheic zone across stream networks. *Hydrological Processes*, *25*, 3525–3532. https://doi.org/10.1002/hyp.8119

Wymore, A. S., Larsen, W., Kincaid, D. W., Underwood, K. L., Fazekas, H. M., Mcdowell, W. H., Murray, D. S., Shogren, A. J., Speir, S. L., & Webster, A. J. (2023). *Revisiting the origins of the power-law analysis for the assessment of concentration-discharge relationships* (pp. 1–17). Water Resources Research. https://doi.org/10.1029/2023WR034910

Zhi, W., Li, L., Dong, W., Brown, W., Kaye, J., Steefel, C., & Williams, K. H. (2019). Distinct source water chemistry shapes contrasting concentration-discharge patterns. *Water Resources Research*, *55*, 4233–4251. https://doi.org/10.1029/2018WR024257

SUPPORTING INFORMATION

Additional supporting information can be found online in the Supporting Information section at the end of this article.

How to cite this article: Warix, S., Navarre-Sitchler, A., & Singha, K. (2024). Water-rock interactions drive chemostasis. *Hydrological Processes*, *38*(2), e15078. https://doi.org/10.1002/hyp.15078